Low-Spin Iron(III) Chiroporphyrins: ^{1}H NMR Studies of Cyanide and Substituted Imidazole Coordination†

Stanisław Wołowiec, Lechosław Latos-Grażyński,* Marinella Mazzanti, and Jean-Claude Marchon*

Department of Chemistry, University of Wrocław, 14 F. Joliot-Curie St., Wrocław 50 383, Poland, and Département de Recherche Fondamentale sur la Matiére Condensée, SCIB/Laboratoire de Chimie de Coordination, CEA Grenoble, F-38054 Grenoble, France

Received May 1, 1997[⊗]

Low-spin complexes of iron(III) chiroporphyrin, obtained from (1*R*)-*cis*-caronaldehyde acid methyl ester and pyrrole as the atropisomer, with R-imidazoles and cyanide have been studied by means of 1D and 2D ^{1}H NMR spectroscopy. A complete spectral assignment of resonances has been done on the basis of observed scalar, NOE, and EXSY correlations in 2D COSY and NOESY experiments. The chemical shift of β-H pyrrole resonances have been used as a sensitive probe of electronic state of iron(III) metal ion. Cyanide anion coordination both in methanol and methylene dichloride results in formation of bis(cyanide) low-spin complexes with the rare $(d_{xz},d_{yz})^4(d_{xy})^1$ electronic ground state, revealed by pyrrole β-H resonances at 11.12 and 10.56 ppm at 293 K, whereas imidazole and 1-methylimidazole produce the bis-ligated complexes with the $(d_{xy})^2(d_{xz},d_{yz})^3$ ground state. In case of sterically hindered imidazole derivatives, i.e., 2-methylimidazole and 1,2-dimethylimidazole, two rotational isomers have been observed at 293 K. Both electronic configurations contribute to the ground state of metal ion for the latter. The steric bulkiness of 2-methylimidazole (or 1,2-dimethylimidazole) is required to freeze a favorable configuration, even at room temperature, providing the perpendicular orientation of two imidazole planes which seems to be instrumental in the stabilization of the rare $(d_{xz}d_{yz})^4(d_{xy})^1$ electronic state.

Introduction

Our approach to produce an asymmetric metalloporphyrin catalyst[1] is to attach bulky substituents on chiral centers near the plane of the tetrapyrrolic ring, as close as possible to the metal atom to maximize steric interaction with incoming substrate. We have shown that a chiroporphyrin catalyst possessing these topological features can be easily constructed from a chiral cyclopropanecarbaldehyde derivative.[2] The prototypic tetramethylchiroporphyrin, $TMCPH_2$, can be obtained from (1*R*)-*cis*-caronaldehydic acid methyl ester[3] and pyrrole as the desired D_2-symmetric $\alpha\beta\alpha\beta$ atropisomer, which exhibits a cleft along a *meso* diagonal on each face of the macrocycle. This chiroporphyrin unit possesses multipoint binding properties with potentially important applications in chiral recognition of axial ligands (Chart 1).

Thus, the ruthenium(II) complex (TMCP)Ru^{II}(CO) demonstrates enantioselective binding of chiral aliphatic alcohols, which results from different van der Waals contacts with the *n*-alkyl substituents for each enantiomer.[4] On the other hand,

Chart 1

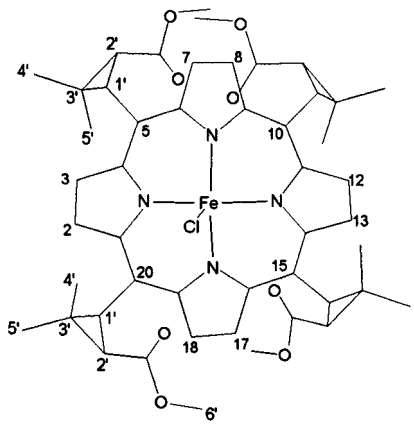

the cobalt(III) complex (TMCP)CoCl binds chiral primary amines in an irreversible, nonenantioselective reaction,[5] while the zinc(II) complex of the related *p*-nitrophenylchiroporphyrin undergoes a drastic shape change from an "open" to a "closed" form upon binding of a pyridine base.[6] Taking into account the remarkably different receptor properties of these two d^6 TMCP complexes, we have now extended our studies to the coordination chemistry of d^5 iron(III) chiroporphyrins. In addition to their possible enantioselection properties, these iron complexes are potentially interesting as asymmetric catalysts in epoxidation or hydroxylation processes.[2,7]

We are aware of the fact that a replacement of *meso* aryl substituents of commonly used metallotetrarylporphyrin catalysts

* Authors to whom correspondence should be addressed: L.L.-G., University of Wrocław; J.-C.M., CEA Grenoble.

† Abbreviations used: P, porphyrin dianion; TPP, 5,10,15,20-tetraphenylporphyrin dianion; OEP, octaethylporphyrin dianion; TAP, 5,10,15,20-tetraisopropylporphyrin dianion; TMCP, chiroporphyrin dianion.

⊗ Abstract published in *Advance ACS Abstracts,* November 15, 1997.

(1) For a recent reviews, see: (a) Collman, J. P.; Zhang, X.; Lee, V. J.; Uffelman, E. S.; Brauman, J. I. *Science* **1993**, *261*, 1404. (b) Naruta, Y. In *Metalloporphyrins in Catalytic Oxidations*; Sheldon, R. A., Ed.; Marcel Dekker: New York, 1994; p 241. (c) Campbell, L. A.; Kodadek, T. *J. Mol. Catal. A* **1996**, *113*, 293. (d) Suslick, K. S.; Van Deusen-Jeffries, S. In *Comprehensive Supramolecular Chemistry*; Atwood, J. L., Davies, J. E. D., MacNicol, D. D., Vögtle, F., and Lehn, J. M., Eds.; Elsevier: Oxford, U.K., 1996; Vol. 5, p 337.

(2) Veyrat, M.; Maury, O.; Faverjon, F.; Over, D. E.; Ramasseul, R.; Marchon, J. C.; Turowska-Tyrk, I.; Scheidt, W. R. *Angew. Chem., Int. Ed. Engl.* **1994**, *33*, 220.

(3) Veyrat, M.; Fantin, L.; Desmoulins, S.; Petitjean, A.; Mazzanti, M.; Ramasseul, R.; Marchon, J. C.; Bau, R. *Bull. Soc. Chim. Fr.*, In press.

(4) Mazzanti, M.; Veyrat, M.; Ramasseul, R.; Marchon, J. C.; Turowska-Tyrk, I.; Shang, M.; Scheidt, W. R. *Inorg. Chem.* **1996**, *35*, 3733.

(5) Toronto, D.; Sarrazin, F.; Pecaut, J.; Marchon, J. C.; Shang, M.; Scheidt, W. R. *Inorg. Chem.*, submitted for publication.

(6) Mazzanti, M.; Marchon, J. C.; Shang, M.; Scheidt, W. R.; Jia, S.; Shelnutt, J. A. *J. Am. Chem. Soc.*, submitted for publication.

(7) Groves, J. T.; Neuman, R. *J. Am. Chem. Soc.* **1989**, *111*, 2900.

S0020-1669(97)00513-2 CCC: $14.00

by bulky alkyl groups may profoundly influence electronic and catalytic properties of the resulting iron tetralkylporphyrins. Generally sterically demanding groups at the porphyrin periphery introduce an extensive nonplanar distortion of the relatively flexible porphyrin macrocycle.[8−11] Conformationally constrained porphyrins and metalloporphyrins have been proposed as model systems to study the electronic consequences of ring deformations.[12] The conformational flexibility of the porphyrin macrocycle has been considered as means of control of redox, spectroscopic, and catalytic properties of metalloenzymes or metalloporphyrins[12−15] including the electronic structure and chemistry of the ferryl porphyrin cation radicals intermediates involved in catalytic oxidation.[16,17]

^{1}H NMR spectroscopy has been shown to be a uniquely sensitive method for detecting and characterizing iron porphyrins. The hyperfine shift patterns that have been recorded for paramagnetic iron porphyrins are sensitive to the iron oxidation, spin, and ligation state.[18,19] Recently we have examined high-spin iron(III) complexes of chiral porphyrin[20] and the corresponding bis-alcohol adducts characterized by a low-spin ground electronic state which is unusual for such a ligation.[31] In this work we have focused on the low-spin derivatives produced by coordination of cyanide or imidazole derivatives.

Typically the ground electronic state of low-spin iron porphyrins evolves between two extreme cases, i.e. $(d_{xy})^2(d_{xz}d_{yz})^3$ and $(d_{xz}d_{yz})^4(d_{xy})^1$.[21−26] A large variety of axial ligands have been probed in order to elucidate the relation between the ligation and the fine details of the electronic structure.[18,19] In the tetrarylporphyrin series the rare $(d_{xz}d_{yz})^4(d_{xy})^1$ ground electronic state has been stabilized by ligands which are simultaneously weak σ-donors and strong π-acceptors such as *t*-BuNC, 4-CN-Py, and $P(OMe)_2Ph$.[23−25] On the basis of EPR studies, the analogous ground electronic state was assigned to low-spin iron(III) chlorins for any low-spin type ligand.[23b,27] Recently we have proven that the controlled modification of the tetrarylporphyrin periphery by addition of the quinoxaline fragment also results in stabilization of the low-spin iron(III) $(d_{xz}d_{yz})^4(d_{xy})^1$ ground electronic state, even in the presence of the axial cyanide ligand.[28]

In the extensive studies on low-spin bis(R-pyridine)iron(III) tetrarylporphyrins Walker, Scheidt, and co-workers[18,23] have demonstrated that the stabilization of the $(d_{xz}d_{yz})^4(d_{xy})^1$ electronic state is related to a relative perpendicular orientation of two planar axial ligands along with an extensively S_4-ruffled porphyrin core. The planar axial ligands are located in perpendicular planes over the *meso* positions in grooves formed due to the porphyrin distortion from planarity.

Nakamura et al. have shown that the steric interaction between methyl of coordinated 2-methylimidazole and *meso*-isopropyl substituent of iron(III) tetralkylporphyrin or 2-methylbenzimidazole and ortho methyl protons of tetramesitylporphyrin stabilizes this unusual electronic structure.[26] Both species, i.e. $[(TAP)Fe^{III}(2\text{-}MeImH)_2]^+$ and $[(TMP)Fe^{III}(2\text{-}MeBzImH)_2]$,$^+$ demonstrated the pyrrole resonances near or in diamagnetic region which may suggest the contribution of the $(d_{xz}d_{yz})^4(d_{xy})^1$ electronic state.[18]

In light of these investigations the $\alpha\beta\alpha\beta$ atropisomer of tetramethylchiroporphyrin ((1*R*)-*cis*-caronaldehydic acid methyl ester at the *meso* position) seems to be perfectly suited to promote the less common ground state of low-spin iron(III) porphyrins. The *meso* alkyl substituents form a groove on each face of the porphyrin what may stimulate the perpendicular orientations of intrinsically planar axial ligands with their planes located above the *meso* positions although the flexibility of the structure remains to be evaluated. The strongly ruffled configurations of chiral porphyrin, associated with the bulkiness of *meso* substituents, have been established by means of X-ray crystallography for $(TMCP)Ru^{II}(CO)(C_2H_5OH)$ and $(TMCP)Fe^{III}Cl$.[5,6,20]

Here we report a detailed examination of the ^{1}H NMR spectra of a variety of low-spin bis(R-imidazole)iron(III) chiroporphyrin complexes in order to elucidate an impact of the porphyrin structure on the electronic properties of the low-spin iron(III) complexes.

Results and Discussion

Symmetry Analysis. The stereochemistry of equatorially coordinated chiroporphyrin $(TMCP)Fe^{III}X_2$ (X = axial ligand) can be anticipated by considering the X-ray structures of $(TMCP)Ru^{II}(CO)(EtOH)$ and $(TMCP)Fe^{III}Cl$.[6,20] There the cyclopropyl substituents of the ruffled porphyrin are oriented alternatively toward either face of the macrocycle. The *cis* configuration of ester and porphyrin groups on each cyclopropane constrains the methyl ester groups to lie on the porphyrin ring, with carbonyl oxygen atoms nearly eclipsing four pyrrole carbon atoms. One methyl of the *gem*-dimethyl group in each cyclopropane also lies over the porphyrin ring, thus defining a C_2-symmetric deep groove of ca. 3−4 Å width along the $C_{meso}-C_{meso}$ axis.

(8) (a) Barkigia, K. M.; Berber, M. D.; Fajer, J.; Medforth, C. J.; Renner, M. W.; Smith, K. M. *J. Am. Chem. Soc.* **1990**, *112*, 8851. (b) Medforth, C. J.; Senge, M. O.; Smith, K. M.; Sparks, L. D.; Shelnutt, J. A. *J. Am. Chem. Soc.* **1992**, *114*, 9859. (c) Senge, M. O.; Medforth, C. J.; Sparks, L. D.; Shelnutt, J. A.; Smith, K. M. *Inorg. Chem.* **1993**, *32*, 1716. (d) Ema, T.; Senge, M. O.; Nelson, N. Y.; Ogoshi, H.; Smith, K. M. *Angew. Chem., Int. Ed. Engl.* **1994**, *33*, 1879. (e) Jentzen, W.; Simpson, M. C.; Hobbs, J. D.; Song, X.; Ema, T.; Nelson, N. Y.; Medforth, C J.; Smith, K. M.; Veyrat, M.; Mazzanti, M.; Ramasseul, R.; Marchon, J.-C.; Takeuchi, T.; Goddard, W. A., III; Shelnutt, J. A. *J. Am. Chem. Soc.* **1995**, *117*, 11085.
(9) Takeda, J.; Sato, M. *Tetrahedron Lett.* **1994**, *35*, 3565.
(10) Mandon, D.; Ochsenbein, P.; Fischer, J,; Weiss, R.; Jayraj, K.; Austin, R. N.; Gold, A.; White, P. S.; Brigaud, O.; Battioni, P.; Mansuy, D. *Inorg. Chem.* **1992**, *31*, 2044.
(11) DiMagno, S. G.; Wersching, A. K.; Ross, I. C. R. *J. Am. Chem. Soc.* **1995**, *117*, 8279.
(12) Barkigia, K. M.; Chantranupong, L.; Smith, K. M.; Fajer, J. *J. Am. Chem. Soc.* **1988**, *110*, 7566.
(13) Eschenmoser, A. *Ann. N.Y. Acad. Sci.* **1986**, *471*, 108.
(14) Geno, M.; Halpern, J. *J. Am. Chem. Soc.* **1987**, *109*, 1238.
(15) Plato, M.; Möbius, K.; Michele-Beyerle,M. E.; Bixon, M. E.; Jortner, J. *J. Am. Chem. Soc.* **1988**, *110*, 7279.
(16) Tsuchiya, S. *J. Chem. Soc., Chem. Commun.* **1991**, 716.
(17) Ochsenbein, P.; Mandon, D.; Fischer, J.; Weiss, R.; Austin, R. N.; Jayraj, K.; Gold, A.; Terner, J.; Bill, E.; Muether, M.; Trautwein, A. X. *Angew. Chem., Int. Engl. Ed.* **1993**, *32*, 1437.
(18) Walker, F. A.; Simonis, U. In *Biological Magnetic Resonance, Volume 12 NMR of Paramagnetic Molecules*; Berliner L. J., Reuben, J., Eds.; Plenum Press: New York, 1993; p 133.
(19) La Mar, G. N.; Walker, F. A. *The Porphyrins*; Dolphin, D., Ed.; Academic Press: New York, 1979; pp 61−312.
(20) Wołowiec, S.; Wojaczyński, J.; Latos-Grażyński, L.; Marchon, J.-C.; Scheidt, W. R.; et al. Unpublished results.
(21) Dugad L. B.; Medhi, O. K.; Mitra, S. *Inorg. Chem.* **1987**, *26*, 1741.
(22) Scheidt, W. R.; Geiger, D. K.; Lee, Y. J.; Reed, C. A.; Lang, G. *Inorg. Chem.* **1987**, *26*, 1039.
(23) (a) Safo M. K.; Walker F. A.; Raitsimiring, A. M.; Walters, W. P.; Dolata, D. P.; Debrunner, P. G.; Scheidt, W. R. *J. Am. Chem. Soc.* **1994**, *116*, 7760. (b) Cheesman, M.; Walker, F. A. *J. Am. Chem. Soc.* **1996**, *118*, 7373. (c) Walker, F. A.; Nasri, H.; Turowska-Tyrk, I.; Mohanrao, K.; Watson, C. T.; Shokhirev, N. V.; Debrunner, P. G.; Scheidt, W. R. *J. Am. Chem. Soc.* **1996**, *118*, 12109.
(24) Simonneaux, G.; Hindre, F.; Le Plouzennec, M. *Inorg. Chem.* **1989**, *28*, 825.
(25) Guillemot, M.; Simmoneaux, G. *J. Chem. Soc., Chem. Commun.* **1995**, 2093.
(26) (a) Nakamura, M.; Ikeue, T.; Neya, S.; Funasaki, N.; Nakamura, N. *Inorg. Chem.* **1996**, *35*, 3731. (b) Nakamura, M.; Nakamura, M. *Chem. Lett.* **1991**, 1885.
(27) (a) Stolzenberg, A. M.; Strauss, S. H.; Holm, R. H. *J. Am. Chem. Soc.* **1981**, *103*, 4763. (b) Coulter, E. D.; Sono, M.; Chang, C. K.; Lopez, O.; Dawson, J. H. *Inorg. Chim. Acta* **1995**, *240*, 603.
(28) Wojaczyński, J.; Latos-Grażyński, L.; Głowiak, T. *Inorg. Chem.*, in press.

Molecular mechanics calculations have been used to visualize the representative structures. In a minimization procedure we have used the standard MM+ parameterization of the Hyperchem program with an exception for the iron coordination surrounding where we have imposed constraints on bond distances consistent with the low-spin iron(III) state.[29,30] As a starting point of molecular mechanics calculations the X-ray-determined structure of a high-spin iron(III) chiroporphyrin has been applied.[20] The planar axial ligands have been initially located in the prearranged equatorial ligand grooves perpendicularly to each other over the $C_{meso}-C_{meso}$ lines. The originally D_2 symmetry of a [(TMCP)Fe^{III}] fragment can be lowered considerably due to the axial coordination.

For the sake of systematization the axial ligands can be classified depending on their intrinsic symmetry as follows: cylindrical, C; planar, C_2-symmetrical with respect to the coordination axis, S_p; planar asymmetrical, A_p; nonplanar asymmetrical, A. Therefore, the low-spin iron(III) chiroporphyrin complexes will fit in the types (TMCP)$Fe^{III}(C)_2$, (TMCP)$Fe^{III}(S_p)_2$, (TMCP)$Fe^{III}(A_p)_2$, (TMCP)$Fe^{III}(A_p)(C)$, and (TMCP)$Fe^{III}(A)_2$ with respect on the axial ligand symmetry (only those combinations are given which were detected in the course of our investigations). To probe the low-spin complexes we have used the following ligands (in parentheses their classifications for the dynamically rigid structures are given): cyanide (C), 1-methylimidazole, 1-MeIm, and imidazole, ImH (S_p), 2-methylimidazole, 2-MeImH, and 1,2-dimethylimidazole, 1,2-diMeIm (A_p), and previously investigated[31] methanol (A). Schematic views of the representative structures of [(TMCP)-Fe^{III}(1,2-diMeIm)$_2$]$^+$ as obtained by molecular mechanics are presented in Figure 1. Complexes are shown in two essential projections presenting the top and side views of the chiroporphyrin. The point symmetry of each species and the predicted number of ^{1}H resonances are collected in Table 1.

One-Dimensional ^{1}H NMR Studies of Low-Spin Iron(III) Chiroporphyrin. The NMR spectra of six-coordinate low-spin iron(III) chiroporphyrins have been analyzed in the context of the symmetry resulting from the axial ligation. Addition of an excess of potassium cyanide to a solution of (TMCP)Fe^{III}Cl in methanol-d_4 results in its conversion to a six-coordinate low-spin complex: [(TMCP)$Fe^{III}(CN)_2]^-$. A titration of (TMCP)Fe^{III}Cl with (TBA)CN in dichloromethane-d_2 produced [(TMCP)$Fe^{III}(CN)_2]^-$ as well. Usually low-spin iron(III) porphyrins, formed by coordination of two cyanide ligands, result in very narrow, paramagnetically shifted resonances due to the optimal relaxation properties.[32] The representative ^{1}H NMR spectra for [(TMCP)$Fe^{III}(CN)_2]^-$ are shown in Figure 2.

The peculiar sets of two downfield-shifted pyrrole resonances at 13.7 and 13.2 ppm (at 233 K in methanol-d_4) is of importance to describe the electronic structure. These resonances are accompanied by a strongly downfield shifted 1′-H resonance and a group of four remaining *meso*-alkyl resonances crowded in the diamagnetic region. A comparison of the spectra collected in dichloromethane-d_2 and methanol-d_4 reveals substantial differences in isotropic shifts. Particularly, a spectacular sign reversal of isotropic shift of pyrrole resonances is observed, which can be accounted for by hydrogen bonding which is present in methanol but is absent in dichloromethane. It was already demonstrated that hydrogen bonding to the cyanide ligand caused general decrease of the [(TPP)$Fe^{III}(CN)_2]^-$ isotropic shifts.[32a] Recently this observation has been attributed to the increasing contribution of the $(d_{xz}d_{yz})^4(d_{xy})^1$ component in the ground electronic state.[18]

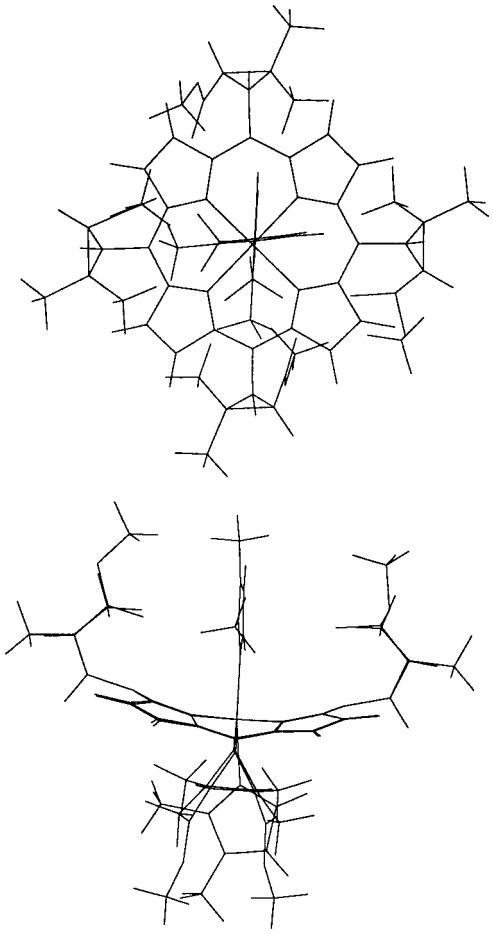

Figure 1. Schematic views of the representative [(TMCP)Fe^{III}(1,2-diMeIm)$_2$]$^+$ structure (isomer *I*) as obtained by molecular mechanics. The complexes are shown in two essential projections presenting the top and side views of the chiroporphyrin.

Table 1. Symmetry-Implicated Multiplicity of ^{1}H NMR Resonances for (TMCP)Fe^{III} Bis-Ligated Complexes

		no. of resonances					
	sym	pyrrole	1-CH	2-CH	4-CH_3	5-CH_3	OCH_3
[(TMCP)Fe^{III}]$^+$	D_2	2	1	1	1	1	1
(TMCP)Fe^{III}(C)[a]	C_2	4	2	2	2	2	2
(TMCP)$Fe^{III}(C)_2$	D_2	2[d]	1	1	1	1	1
(TMCP)$Fe^{III}(S_p)_2$	D_2	2[d]	1	1	1	1	1
(TMCP)$Fe^{III}(A_p)_2I$[b]	C_2	4[e]	2	2	2	2	2
(TMCP)$Fe^{III}(A_p)_2II$[c]	C_2	4[f]	2	2	2	2	2
(TMCP)$Fe^{III}(A_p)(C)$	C_1	8	4	4	4	4	4
(TMCP)$Fe^{III}(A)_2$	C_1	8	4	4	4	4	4

[a] C_2 axis oriented along the iron−cylindric ligand bond. [b] C_2 axis oriented along the $N_{21}-N_{23}$ pyrrole nitrogens. [c] C_2 axis oriented along the $N_{22}-N_{24}$ pyrrole nitrogens. [d] Equivalent pyrrole protons [2-H, 3-H, 12-H, 13-H], [7-H, 8-H, 17-H, 18-H]. [e] Equivalent pyrrole protons [2-H, 3-H], [7-H, 18-H], [8-H, 17-H], [12-H, 13-H]. [f] Equivalent pyrrole protons [2-H, 13-H], [3-H, 12-H], [7-H, 8-H], [17-H, 18-H].

Titration of imidazole or its methylated derivatives to (TMCP)Fe^{III}Br converts high-spin iron chiroporphyrin into the respective low-spin counterparts. The complete conversion has been achieved for a 1:4 (TMCP)Fe^{III}Br:R-imidazole molar ratio even for the most sterically hindered 1,2-diMeIm. In each investigated case we have confirmed the coordination of two R-Im ligands by integration of the pyrrole and R-imidazole ligand resonances. The ^{1}H NMR spectra for a series of [(TMCP)Fe^{III}(R-Im)$_2$]$^+$ complexes are shown in Figure 3. The

(29) Scheidt, W. R.; Lee, Y. J. *Struct. Bonding* **1987**, *64*, 1.
(30) Munro, O. Q.; Marques, H. M.; Debrunner, P. G.; Mohanrao, K.; Scheidt, W. R. *J. Am. Chem. Soc.* **1995**, *117*, 935.
(31) Wojaczyński, J.; Wołowiec, S.; Latos-Grażyński, L.; Simonato, J. P.; Marchon, J.-C. Unpublished results.
(32) (a) La Mar, G. N.; Del Gaudio, J., Frye, J. S. *Biochim. Biophys. Acta* **1977**, *498*, 422. (b) La Mar, G. N.; Viscio, D. B.; Smith, K. M.; Caughey, W. S.; Smith, M. L. *J. Am. Chem. Soc.* **1978**, *100*, 8065.

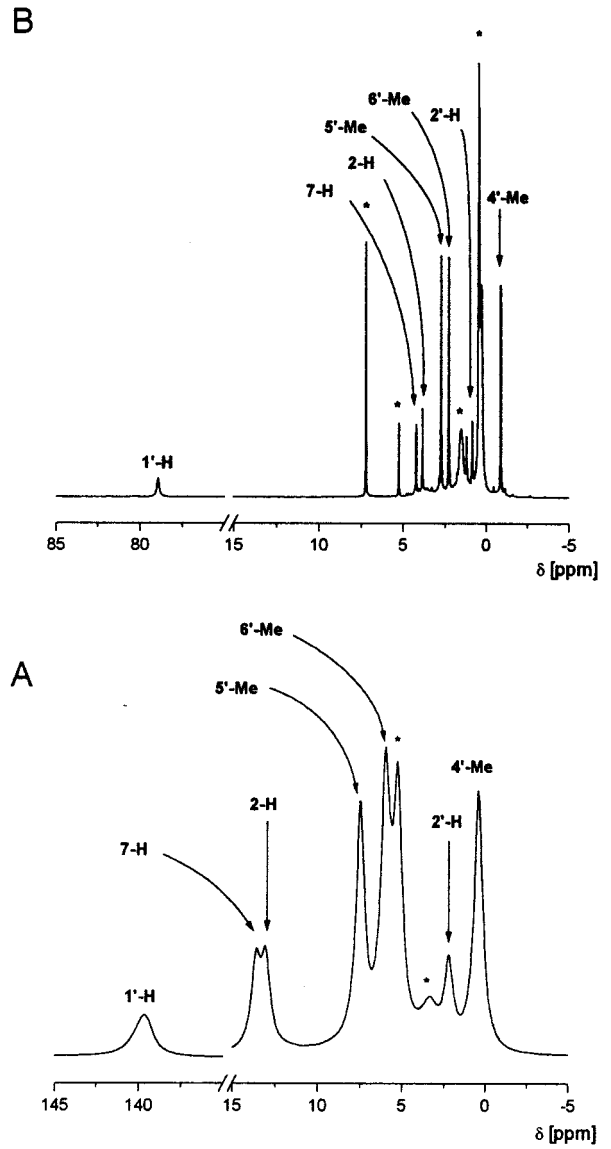

Figure 2. 300 MHz ^{1}H NMR spectra: (A) (TMCP)Fe^{III}(CN)$_2$]$^-$ in methanol-d_4 at 233 K; (B) [(TMCP)Fe^{III}(CN)$_2$]$^-$ in dichloromethane-d_2 at 273 K. Resonance assignments follow those used in the text. In each case, where a group of protons contributes to a single resonance, the label of the representative member for the set is only given. Asterisks indicate solvent (A) or solvent and TBA resonances (B).

resonance assignments which are given above selected peaks have been made on the basis of relative intensities, line width analysis, and 2D NMR experiments. The labeling is made according to Chart 1. In agreement with our classification, which correlates the symmetry of axial ligands and the multiplicity of observed resonances, the generated complexes are assigned to the following categories: (TMCP)Fe^{III}(C)$_2$, [(TMCP)Fe^{III}(CN)$_2$]$^-$; (TMCP)Fe^{III}(S$_p$)$_2$, [(TMCP)Fe^{III}(1-MeIm)$_2$]$^+$, [(TMCP)Fe^{III}(ImH)$_2$]$^+$; (TMCP)Fe^{III}(A$_p$)$_2$-*I* and (TMCP)Fe^{III}(A$_p$)$_2$-*II*, [(TMCP)Fe^{III}(2-MeImH)$_2$]$^+$, [(TMCP)Fe^{III}(1,2-di-MeIm)$_2$]$^+$.

Spectral patterns determined for the less sterically hindered imidazoles (ImH, 1-MeIm) appear, at first, contradictory to the elaborated correlation (Table 1). To reconcile these differences we have to consider a possibility that the ^{1}H NMR experiments do reflect an *effective* symmetry, which for a given system may be higher than predicted solely for a rigid structure. The fast rotation around the Fe−N(R-imidazole) bond generates, as a resultant, the (TMCP)Fe^{III}(S$_p$)$_2$ type spectrum. The steric hindrance of 2-MeImH and 1,2-diMeIm slowed down such a rearrangement to an extent that two isomers gave two well-

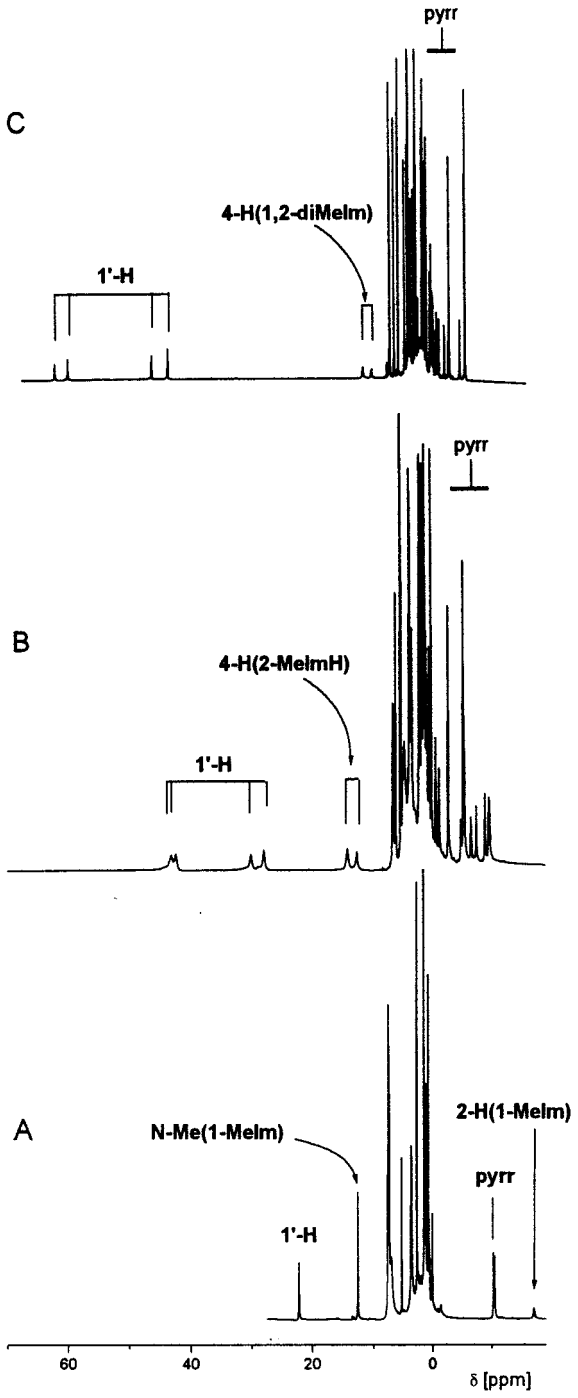

Figure 3. 300 MHz ^{1}H NMR spectra: (A) TMCP)Fe^{III}(1-MeIm)$_2$]$^+$, (B) [(TMCP)Fe^{III}(2-MeImH)$_2$]$^+$, and (C) [(TMCP)Fe^{III}(1,2-diMeIm)$_2$]$^+$ in dichloromethane-d_2 at 273 K. Resonance assignments are as in Figure 2. The crowded region of eight pyrrole resonances is labeled schematically pyrr.

separated sets of resonances corresponding to the (TMCP)Fe^{III}-(A$_p$)$_2$-*I* and (TMCP)Fe^{III}(A$_p$)$_2$-*II* geometry, respectively. We could easily distinguish these sets based solely on the corresponding intensities ratios as their populations are different and temperature dependent.

To complete the overview of all accessible coordination environments we have made an attempt to generate a spectrum corresponding to the (TMCP)Fe^{III}(A$_p$)(C) pattern. Titration of [(TMCP)Fe^{III}(1,2-diMeIm)$_2$]$^+$ with (TBA)CN produces, apart from already characterized [(TMCP)Fe^{III}(CN)$_2$]$^-$, the mixed-ligand complex [(TMCP)Fe^{III}(1,2-diMeIm)(CN)] (Figure 4). This species reveals a predicted spectral pattern of four 1′-H resonances. The pyrrole resonances are partially covered by the TBA countercation lines. Hence a single sterically hindered

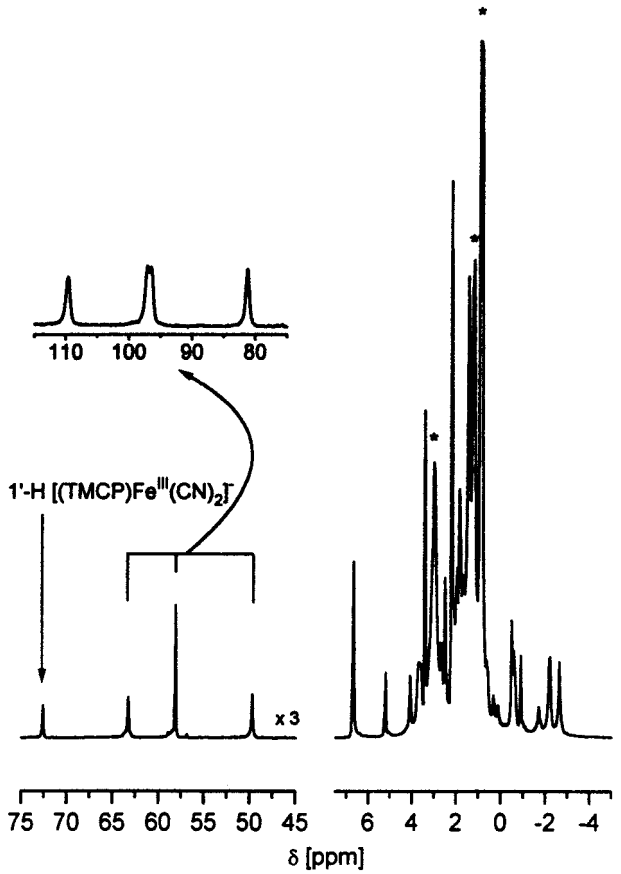

Figure 4. ^{1}H NMR titration of [(TMCP)Fe^{III}(1,2-diMeIm)$_2$]$^+$ with (TBA)CN in dichloromethane-d_2 at 293 K. The spectrum demonstrates the stage ([(TMCP)Fe^{III}]Cl:CN$^-$:1,2-diMeIm molar ratio 1:1.2:2.5) where the mixed-ligand species [(TMCP)Fe^{III}(1,2-diMeIm)(CN)] predominates in the system. The inset demonstrates the fragment of the spectrum at 223 K with four well-separated 1′-H resonances of [(TMCP)Fe^{III}(1,2-diMeIm)(CN)].

ligand induces the porphyrin deformation and generates a barrier of rotation, which is sufficient to stabilize a position of the 1,2-diMeIm plane in the structure.

The effects of temperature on the ^{1}H NMR spectra of [(TMCP)Fe^{III}(CN)$_2$]$^-$ and [(TMCP)Fe^{III}(1,2-diMeIm)$_2$]$^+$ are shown in Figure 5, where the pyrrole and 1′-H chemical shifts are plotted versus 1/*T*. In general these plots are not linear as would be expected according to the Curie law for simple paramagnetic complexes. Rather they show noticeable curvatures. The curvature in Figure 5 can be ascribed to the effects related to the thermal equilibrium between two alternative electronic states $(d_{xy})^2(d_{xz}d_{yz})^3 \leftrightarrow (d_{xz}d_{yz})^4(d_{xy})^1$ of low-spin iron(III) porphyrins (vide infra).

2D NMR Studies of (TMCP)Fe^{III}(S)$_2$ Low-Spin Iron(III) Chiroporphyrin. The complete assignments of resonances required an application of two-dimensional ^{1}H NMR techniques. Routinely the 2D NMR spectra have been collected at several temperatures to achieve the optimal spread of the one-dimensional spectrum prior to two-dimensional analysis. Here we present only the most fundamental steps of the resonance assignments carried out in the representative case of [(TMCP)-Fe^{III}(ImH)$_2$]$^+$ as shown in the combined COSY/NOESY map in Figure 6.

Generally, to simplify the discussion of 2D NMR spectra, we will usually list only one of a set of symmetry-equivalent pairs of protons engaged in exchange or scalar or dipolar coupling (Table 1). The analysis of the structural models of [(TMCP)Fe^{III}(ImH)$_2$]$^+$ predicts that the NOESY spectra may exhibit through-space correlations between the protons in adjacent pyrrole rings, e.g. 2-H−18-H and between the protons

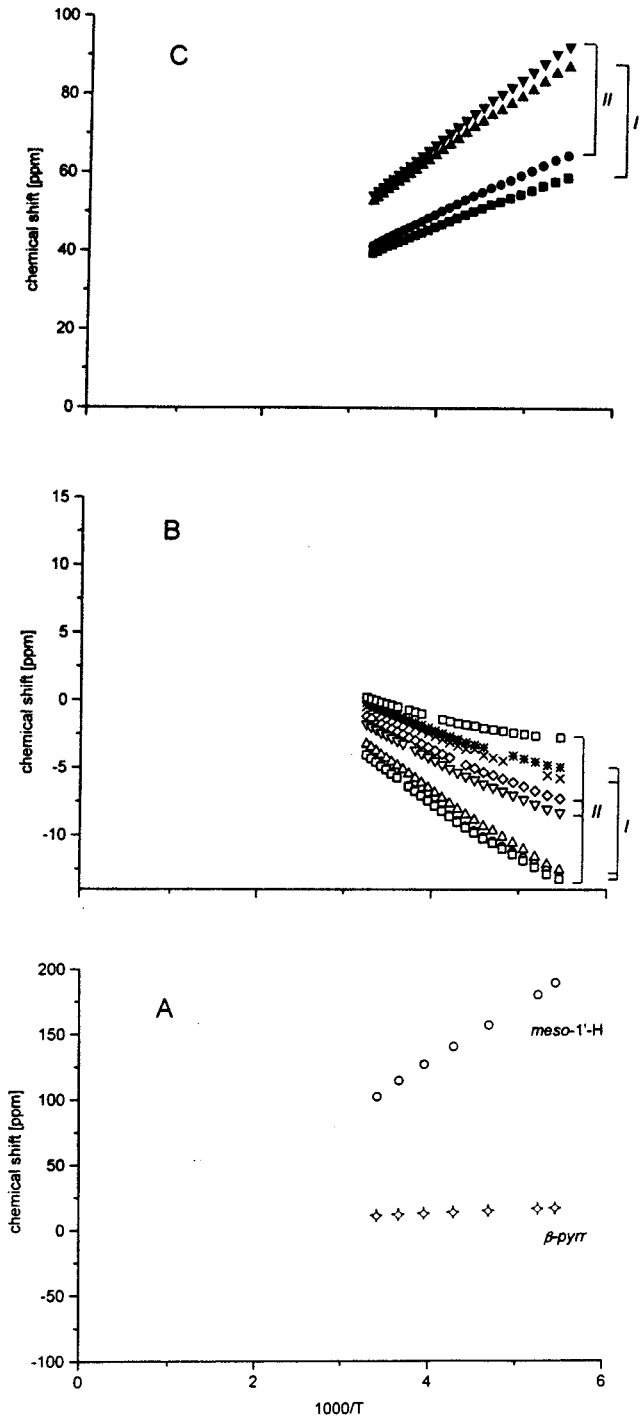

Figure 5. Temperature dependence of the chemical shifts of (A) pyrrole and 1′-CH resonances of [(TMCP)Fe^{III}(CN)$_2$]$^-$ in methanol-d_4 and (B) pyrrole and (C) 1′-CH resonances of [(TMCP)Fe^{III}(1,2-diMeIm)$_2$]$^+$ in dichloromethane-d_2. The individual assignments are shown in the figure.

of pyrrole rings and the *meso* substituents: 3-H−5-(5′-Me), 7-H−5-(2′-H), 3-H−5-(1′-H), and 7-H−5-(1′-H). Eventually we have identified two crucial cross-peaks, **b**, 3-H−5-(5′-Me), and **c,** 7-H−5-(2′-H), which allowed the recognition of 2-H and 7-H in the one-dimensional ^{1}H NMR spectrum (Figure 3, Table 2). Accordingly the resonances at −13.55 and −13.12 ppm (263 K) correspond respectively to the [2-H, 3-H, 12-H, 13-H] and [7-H, 8-H, 17-H, 18-H] groups of pyrrole protons. The spatial contacts within the *meso*-alkyl protons are pronounced via the cross-peak **d** between 1′-H and 5′-Me and two cross-peaks correlating 6′-Me−5′-Me and 4′-Me−6′-Me resonances (not labeled). Additionally, the EXSY peak **e** between the 5-H proton of free and coordinated ImH provided support for the assignment of the axial ligand resonances. The observed COSY/

Table 2. ^{1}H NMR Chemical Shift Data at 293 K for the Studied Complexes

ligand	locant					
	β-pyrrole	4′-Me	5′-Me	6′-Me	1′-H	2′-H
CN^- (KCN in MeOD)	11.12; 10.56 (av 10.84)	0.9	5.31	6.92	101.87	2.76
CN^- ((TBA)CN in $CDCl_3$)	3.57 (7,8,17,18); 3.23 (2,3,12,13) (av 3.40)	−0.65	2.57	[a]	69.12	1.00
1,2-diMeIm						
I[d]	−4.93 (7,8); −4.08 (2,13); −0.99 (3,12); −0.66 (17,18) (av −2.67)	−5.24 (15,20); 2.75 (5,10) (av −1.25)	0.78 (15,20); 2.59 (5,10) (av 1.69)	1.37 (15,20); 5.65 (5,10) (av 3.51)	55.73 (15,20); 41.12 (5,10) (av 48.44)	−0.40 (15,20); 1.95 (5,10) (av 0.78)
II[e]	−4.95 (12,13); −2.44 (8,17); −1.79 (2,3); −0.20 (7,18) (av −2.35)	−2.97 (5,20); 0.42 (10,15) (av −1.28)	1.23 (5,20); 2.29 (10,15) (av 1.76)	3.5 (5,20); 3.5 (10,15) (av 3.5)	57.49 (5,20); 43.37 (10,15) (av 50.43)	−0.99 (5,20); 2.3 (10,15) (av 0.66)
2-MeImH						
I[f]	−7.83; −7.22;[c] −4.11; −4.11[c] (av −5.81)	−4.56; 2.95 (av −0.81)	0.2; 2.07 (av 1.14)	[b]	41.12; 28.1 (av 34.61)	−0.55; 2.2 (av 0.83)
II[g]	−7.83; −5.94;[c] −5.08; −3.72[c] (av −5.64)	−2.44; 0.96 (av −0.74)	0.56; 1.69 (av 1.13)		41.77; 29.95 (av 35.86)	−1.17; 1.77 (av 0.30)
1-MeIm[h]	−8.31 (2,3,12,13); −8.18 (7,8,17,18) (av −8.25)	0.52	1.57	2.88	23.96	0.36
ImH[i]	−10.16 (2,3,12,13); −9.97 (7,8,12,18) (av −10.07)	0.3	0.96	3.54	15.83	0.53

[a] Not assigned. [b] Not assigned at 293 K. [c] Connected to each to other via scalar cross-peak in the COSY spectrum. [d−i]The axial base resonances were identified as follows: (*d*) 0.26 (2-Me), 9.49 (4-H), −0.32 (5-H), 4.15 ppm (N-Me); (*e*) 0.52 (2-Me), 8.21 (4-H), −0.82 (5-H), 3.74 ppm (N-Me); (*f*) 11.77 ppm (4-H); (*g*) 10.49 ppm (4-H); (*h*) −15.68 (2-H), −1.64 (5-H), 11.04 ppm (N-Me); (*i*) −14.41 (2-H), 2.02 (4-H), 1.24 ppm (5-H).

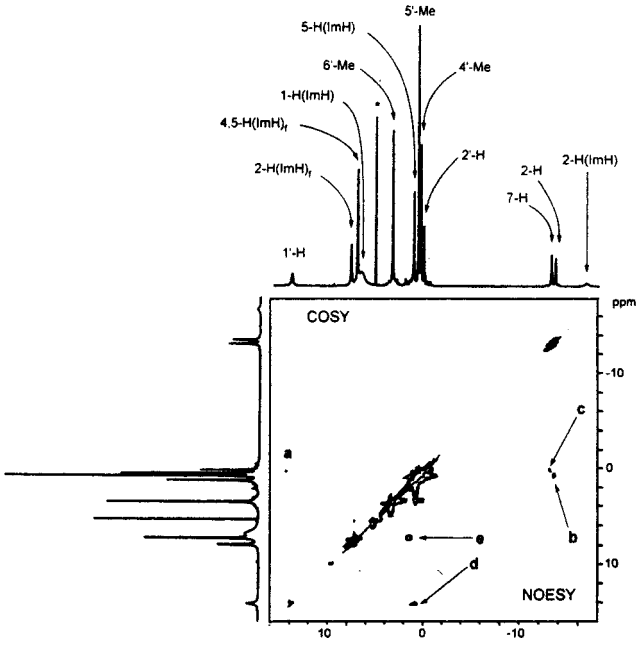

Figure 6. 2D ^{1}H NMR spectra of $[(TMCP)Fe^{III}(ImH)_2]^+$ in dichloromethane-d_2 at 263 K. The upper left triangle presents the COSY map, and the bottom-right part demonstrates the NOESY experiment. The most characteristic cross-peaks are labeled as follows. COSY: **a**, 1′-H−2′-H. NOE: **b**, 3-H−5-(5′-Me) (equivalent to (2-H−20-(5′-Me)); **c**, 7-H−5-(2′-H); **d**, 1′-H−5′-Me. EXSY: **e**, 5-H(ImH)$_f$−5-H(ImH).

NOESY pattern of cross-peaks is fairly reproducible for all other systems studied here. The 2-H−5′-Me and 7-H−2′-H cross-peaks in relevant NOESY maps are of particular importance and can be considered further as a convenient starting point in the spectroscopic analysis. They were observed for other systems of the $(TMCP)Fe^{III}(C)_2$ and $(TMCP)Fe^{III}(S)_2$ symmetry types, i.e. $(TMCP)Fe^{III}(CN)_2]^-$ and $[(TMCP)Fe^{III}(1\text{-}MeIm)_2]^+$, respectively, as well as for the systems with restricted rotation around the axial coordination bond (2-MeImH, 1,2-diMeIm).

2D NMR Studies of $(TMCP)Fe^{III}(A)_2$ Low-Spin Iron(III) Chiroporphyrin. The relatively simple case of $[(TMCP)Fe^{III}(ImH)_2]^+$ has established a background for the analysis of the more elaborate situation encountered for $[(TMCP)Fe^{III}(2\text{-}MeImH)_2]^+$ and $[(TMCP)Fe^{III}(1,2\text{-}diMeIm)_2]^+$. As a matter of fact, we have used the $[(TMCP)Fe^{III}(ImH)_2]^+$ complex to search for optimal conditions of NOESY experiments which would be appropriate for low-spin $[(TMCP)Fe^{III}(R\text{-}Im)_2]^+$ complexes in general. The observation of the NOE cross-peaks for the low-spin bis(R-imidazole)iron(III) porphyrins depends strongly on the selection of the experimental parameters, i.e. a mixing time, the block size, and the spectral bandwidth. Their values are determined by intrinsic properties of the investigated species as expressed by the relevant T_1 and T_2* values. In general we have followed the recipes elaborated for bis(R-imidazole)iron(III) tetraarylporphyrins by Simonis, Walker, and co-workers[33] as a guidelines for the parameter choice (the acquisition time in $t_2 \sim 1.5T_1$; the acquisition time in $t_1 \sim (1/2)t_2$; τ_m $1.15-1.3T_1$ of the shortest T_1 of the coupled pair). Approximate T_1 relaxation times for pyrrole resonances of $[(TMCP)Fe^{III}(1,2\text{-}diMeIm)_2]^+$ equal 50 ms. Apparently, the relaxation times are favorable for NOE correlations in comparison to previously investigated sterically hindered bis(R-imidazole) low-spin iron(III) tetrarylporphyrins.[33]

Figure 7 presents NOESY/COSY spectra of $[(TMCP)Fe^{III}(2\text{-}MeImH)_2]^+$ collected at 273 K. Previously in the one-dimensional spectra we have unambiguously identified two well-defined subsets of resonances assigned to two isomers. Within each nonequivalent pyrrole ring the pyrrole protons are expected to be scalarly coupled with an approximate 5 Hz coupling constant. Cross-peaks on the COSY map (the lower fragment of Figure 7) reveal pairwise scalar coupling between symmetry-unequivalent protons located on the same pyrrole ring i.e. (2,3), (12,13) for the isomer $[(TMCP)Fe^{III}(2\text{-}MeImH)_2]^+$-*I* and (7,8), (17,18) for the isomer $[(TMCP)Fe^{III}(2\text{-}MeImH)_2]^+$-*II*. Thus, the pyrrole resonances without scalar correlation to any other pyrrole resonance could be unambiguously assigned to two other pyrrole rings for each isomer. Characteristic sets of cross-peaks due to coupling between protons of each alkyl substituent have been

(33) (a) Walker, F. A.; Simonis, U. *J. Am. Chem. Soc.* **1991**, *113*, 8652. (b) Lin, Q.; Simonis, U.; Tipton, A. R.; Norvell, C. J. Walker, F. A. *Inorg. Chem.* **1992**, *31*, 4216. (c) Simonis, U.; Dallas, J.; Walker, F. A. *Inorg. Chem.* **1992**, *31*, 5349. (d) Simonis, U.; Lin, Q.; Tan, H.; Barber, R. A.; Walker, F. A. *Magn. Res. Chem.* **1993**, *31*, S133. (e) Tan, H.; Simonis, U.; Shokiriev, N. V.; Walker, F. A. *J. Am. Chem. Soc.* **1994**, *116*, 5784.

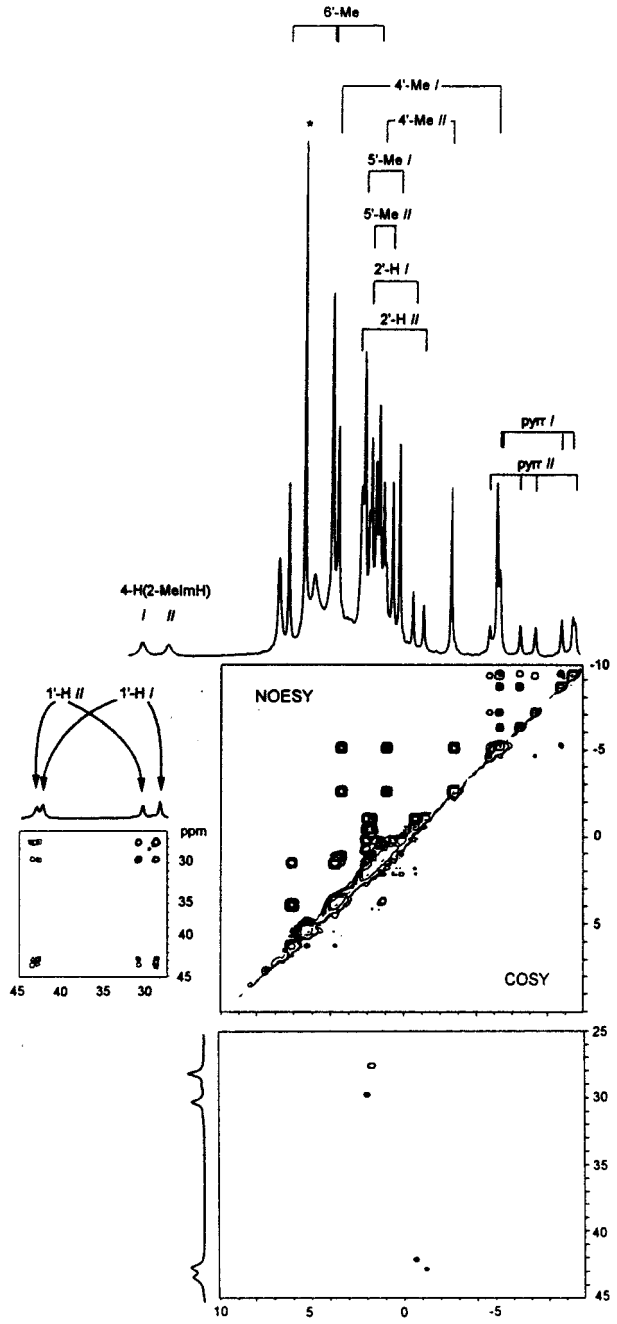

Figure 7. 2D ^{1}H NMR spectra of $[(TMCP)Fe^{III}(2\text{-MeImH})_2]^+$ in dichloromethane-d_2 at 273 K. The two upper fragments present the NOESY map, and the two bottom ones demonstrate the COSY experiment. Resonance assignments shown in the one-dimensional projections follow those in text.

established and located in the COSY map for two pairs of unequivalent *meso*-alkyl substituents.

The complementary peak assignments have been derived from the NOESY and ROESY experiments. The NOESY map for $[(TMCP)Fe^{III}(2\text{-MeImH})_2]^+$ collected at 273 K is presented at left upper triangle in Figure 7. At that temperature the five groups of EXSY cross-peaks between β-pyrrole resonances (−4 to −10 ppm), 4′-Me (-6 to 4 ppm), 5′-Me (0 to 2 ppm), 6′-Me (2 to 6.5 ppm, peaks not labeled), 1′-H (28 to 44 ppm, left inset), and 2′-H (-1.2 to 2.1 ppm) were observed and, with the supporting information on their relative intensity, allowed to separate the porphyrin resonances into subsets corresponding to two isomers *I* and *II* (see labeling at Figure 7).

In case of the more sterically hindered imidazole derivative, i.e. 1,2-diMeIm, the COSY experiment at 293 K provided the unambiguous assignments of 2′-H resonances due to observed

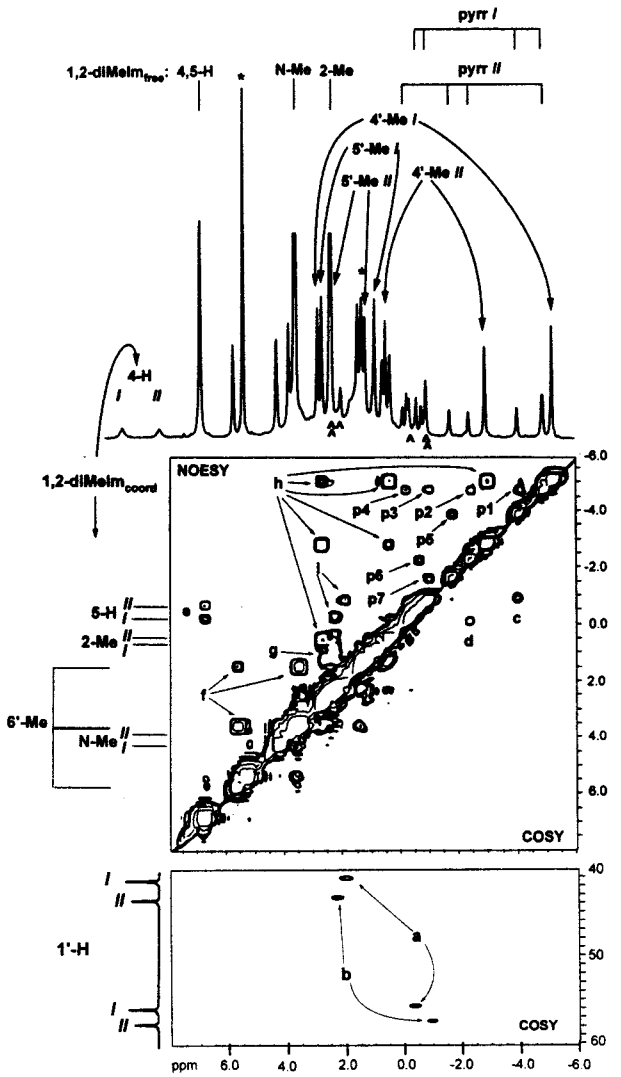

Figure 8. 2D ^{1}H NMR spectra of $[(TMCP)Fe^{III}(1,2\text{-diMeIm})_2]^+$ in dichloromethane-d_2 at 293 K. The upper left triangle presents the NOESY map, and the two bottom parts demonstrate the COSY experiment. The most characteristic cross-peaks are labeled as follows. COSY: **a**, 1′-H^{II}−2′-H^{I}. NOE: **b**, 1′-H^{II}−2′-H^{II}; **c**, 2-H^{I}−3-H^{I}, **d**, 7-H^{II}−8-H^{II}. EXSY: 6′-Me (**f**), 5′-Me (**g**), 4′-Me(**h**), 2′-H (**i**). The **p1**−**p7** cross-peaks reflect EXSY correlation between pyrrole resonances of two isomers. Resonance assignments shown in the one-dimensional projections are as in the text. The 2′-H^{I} and 2′-H^{II} resonances are labeled with ∧ and double ∧, respectively, under the 1D projection.

scalar 1′-H−2′-H connectivities revealed by **a** and **b** cross-peaks for the *I* and *II* isomers, respectively (lower part of COSY map in Figure 8). Cross-peaks **c** and **d** demonstrate pairwise scalar coupling between symmetry unequivalent pyrrole protons located on the same pyrrole ring, i.e. (7-H−8-H), (17-H−18-H) for the isomer *I* and (2-H−3-H), (12-H−13-H) for the isomer *II*.

We have observed that temperature effects play a crucial role in the NOESY map obtained. Apart from NOE-related resonances one can expect EXSY cross-peaks due to two dynamic phenomena, i.e. an axial ligand exchange between free and coordinated 1,2-diMeIm and a hindered rotation of coordinated R-imidazoles with respect to the Fe−N(imidazole) axis. Accordingly the very intense EXSY cross-peaks are observed between all four resonances of each particular set assigned to the respective *meso*-alkyl positions: 6′-Me (**f**), 5′-Me (**g**), 4′-Me (**h**), 2′-H (**i**), and 1′-H (observed but not shown). These correlations are created by the internal rotation. The group of eight pyrrole resonances demonstrates a more complicated picture of mutual correlations demonstrating seven **p1**−**p7** cross-

peaks. The missing cross-peak between two the most downfield shifted resonances of similar intensity is presumably hidden under the diagonal trace. Four other cross-peaks of lower intensity could be also observed at the lower threshold (not shown). For the suggested rearrangement process one can anticipate EXSY peaks which internally correlate two pyrrole resonances of a single isomer. Furthermore the external correlation between two isomeric forms is accessible as well. Each pyrrole resonance which is not scalar coupled, as determined previously in the COSY map, reveals one internal correlation, i.e. one cross peak to the other singlet from the same isomer, and two external corrections, i.e. two cross peaks to a pair of scalar coupled pyrrole resonances identified with the second isomer. In addition, a set of three cross peaks between one component of a scalar coupled pair incorporate two external EXSY peaks with two singular pyrrole resonances of the other isomer and the internal cross peak between the proton resonances located on the same pyrrole ring. Because of their spatial proximity the combination of the EXSY and NOE effects can be essential in this case. The ROESY experiment carried out at 293 K (the map not shown) gave identical qualitative results as NOESY. At the NOESY map collected at 293 K we have also observed the EXSY cross-peaks **e** between free and coordinated 1,2-diMeIm. Such an exchange is typical for low-spin iron(III) porphyrins.[26,33d,34−36] We have found it useful to apply this correlations as effective means of a straightforward assignment of 5-H(1,2-diMeIm) related to coordinated 1,2-diMeIm.

Gradually decreasing the temperature, we were able to follow systematically positions of all the resonances and to partially suppress the EXSY cross-peaks providing finally the appropriate conditions for observation of the NOE effects in the NOESY experiment. This goal has been achieved at 190 K at excess of 1,2-diMeIm ligand (3:1 1,2-diMeIm:(TMCP)Fe^{III}Br molar ratio). The relevant fragment of NOESY map is presented at Figure 9. The relays of the established NOE connectivities are shown in Figure 10. The cross-peaks labeled **a**−**h** are related to the isomer *I*. The 2-H−3-H couple demonstrated scalar coupling throughout the entire range of temperature (COSY spectra were taken at four temperatures between 293 and 190 K). Their assignments have been independently confirmed by NOE cross-peaks **a** and **e** which correspond to the 2-H^{I}−20-(5′-$Me)^{I}$ and 3-H^{I}−5-(5′-$Me)^{I}$ dipolar correlations. The estimated distances, as found from the molecular model, between pyrrole 2-H and 3-H protons and located in the plane of the porphyrin core 20-(5′-Me) and 5-(5′-Me) protons are equal 3.51 and 3.43 Å, whereas those between 2-H and 3-H and located over the porphyrin macrocycle 20-(4′-Me) and 5-(4′-Me) protons are equal to 3.47 and 3.48 Å, respectively. The NOE cross-peaks **b**−**d**, **g**, and **h** within the 15-*meso*-alkyl substituents were observed as well. The 5-substituent resonances were assigned by default. Two other spatial contacts between 17-H−15-(2-H′) (**f**) and 7-H− 5-(2′-H) (**i**) (not shown at Figure 9 but observed at the lower threshold) completed the pyrrole/periphery NOE correlation pattern. The estimated distances between mentioned pyrrole and 2′-H protons are equal to 2.73 and 2.81 Å, respectively. Unfortunately, presumably due to substantial difference in T_1 relaxation times between the 2-Me resonances of axial ligand and porphyrin protons we have not identified the essential cross-peaks which would point to the spatial proximity between the selected fragments of the complex. Consequently, it precludes the unambiguous determination of the 1,2-diMeIm ligand orientation with respect to the porphyrin skeleton.

The spread of resonances within the isomer *II* is smaller, and eventually we have observed the 2-H−20-(4′-Me) (**k**) and 2-H−20-(5′-Me) (**l**) spatial contacts. The complete connectivity of 5- (or 20-) *meso*-alkyl substituent via the **m**−**q** relay has been achieved in case of that isomer. An additional cross-peak **r** (not shown) between 10-(2′-H) and 10-(4′-Me) confirmed the assignment of peripheral resonances. Two other NOE cross-peaks (**sI** and **sII)** between N-Me and 2-Me of coordinated ligand were observed for isomers *I* and *II*, respectively. The chemical exchange was not completely suppressed in the studied system, and the EXSY as well as combined EXSY/NOE cross-peaks were found at 190 K (those are not marked at the Figure 9).

Rearrangements of Low-Spin Iron(III) Chiroporphyrins. The rotation of 1,2-diMeIm or 2-MeImH although relatively slow, as we can see the separate sets of resonance for two rotamers in the very large (183−303 K) temperature range, has been confirmed by EXSY resonances at the NOESY spectra (Figures 7 and 8). These are the very first examples of such a stability in the low-spin iron(III) porphyrin series. Previously it has been reported that coordination of sterically hindered imidazoles to form $[(TMP)Fe^{III}(2\text{-}MeImH)_2]^+$,[33a,37a] $[(TMP)Fe^{III}(2\text{-}MeBzIm)_2]^+$,[37b] and $[(TAP)Fe^{III}(2\text{-}MeImH)_2]^+$ [26] induced the S_4 deformation and froze the rotation around the Fe−N bond but only in low-temperature limits.

We assume that the dynamic rearrangement of the otherwise sterically hindered chiroporphyrins require the intermediate form which would facilitate the exchange between $[(TMCP)Fe^{III}(1,2\text{-}diMeIm)_2]^+$ isomers. The alternative ruffled structure, which takes an advantage of the fact that the fence is enlarged only on one face of the porphyrin, is presented in Figure 11. The rotation will create successive switching of the up/down ruffling distortion at the particular *meso* positions and will be accompanied by the displacement of the chiral alkyl substituent outward of the porphyrin pocket extending its diameter. Such a sequence of porphyrin rearrangements may facilitate the concerted rotation which preserves the 90° 1,2-diMeIm−1,2-diMeIm dihedral angle. Less sterically hindered 1-MeIm or ImH ligands are not bulk enough to restrain the rotation. It is tempting to treat this observation in terms of the analogous mechanism as for 1,2-diMeIm, i.e. to include an exchange between two more stable rotamers via intermediate structures although with a smaller activation energy than for 1,2-diMeIm. However one cannot exclude a possibility that an extent of ruffling in $[(TMCP)Fe^{III}(ImH)_2]^+$ ($[(TMCP)Fe^{III}(1\text{-}MeIm)_2]^+$) is much smaller allowing an unhindered dynamic process. In the relevant comparison, the strongly ruffled porphyrin cores were determined for $[(TMP)Fe^{III}(2\text{-}MeImH)_2]^+$ [30] and $[(TPP)Fe(2\text{-}MeImH)_2]^+$,[38] but almost planar porphyrin cores were observed for related examples $[(OEP)Fe^{III}(2\text{-}MeImH)_2]^+$ [39] and $[(TMP)Fe^{III}(1\text{-}MeIm)_2]^+$.[40] There the steric interaction was partially released either by removing the *meso* substituents but preserving the axial ligand, $[(OEP)Fe^{III}(2\text{-}MeImH)_2]^+$, or by removing 2-$CH_3$ group from the axial ligand for the same bulky porphyrin, $[(TMP)Fe^{III}(1\text{-}MeIm)_2]^+$. The recent analysis of

(34) Walker, F. A.; Simonis, U.; Zhang, H.; Walker, J. M.; McDonald Ruscitti, T.; Kipp, C.; Amptuch, M. A.; Castillo, B. V., III; Cody, S. H.; Wilson, D. L.; Graul, R. E.; Yong, G. J.; Tobin, K.; West, T. J.; Barichiewich, B. A. *New. J. Chem.* **1992**, *16*, 609.
(35) Nakamura, M.; Tajima, K.; Tada, K.; Ishizu, K.; Nakamura, N. *Inorg. Chim. Acta* **1994**, *224*, 113.
(36) Saterlee, J. D.; La Mar, G. N.; Bold, T. J. *J. Am. Chem. Soc.* **1977**, *99*, 1088.
(37) (a) Nakamura, M.; Groves, J. T. *Tetrahedron* **1988**, *44*, 3225. (b) Nakamura, M. *Bull. Chem. Soc. Jpn.* **1995**, *68*, 197.
(38) Scheidt, W. R.; Kiner, J. F.; Hoard, J. L.; Reed, C. A. *J. Am. Chem. Soc.* **1987**, *109*, 1963.
(39) Geiger, D. K.; Lee, Y. J.; Scheidt, W. R. *J. Am. Chem. Soc.* **1984**, *106*, 6339.
(40) Safo, M. K.; Gupta, G. P.; Walker, F. A.; Scheidt, W. R. *J. Am. Chem. Soc.* **1991**, *113*, 5497.

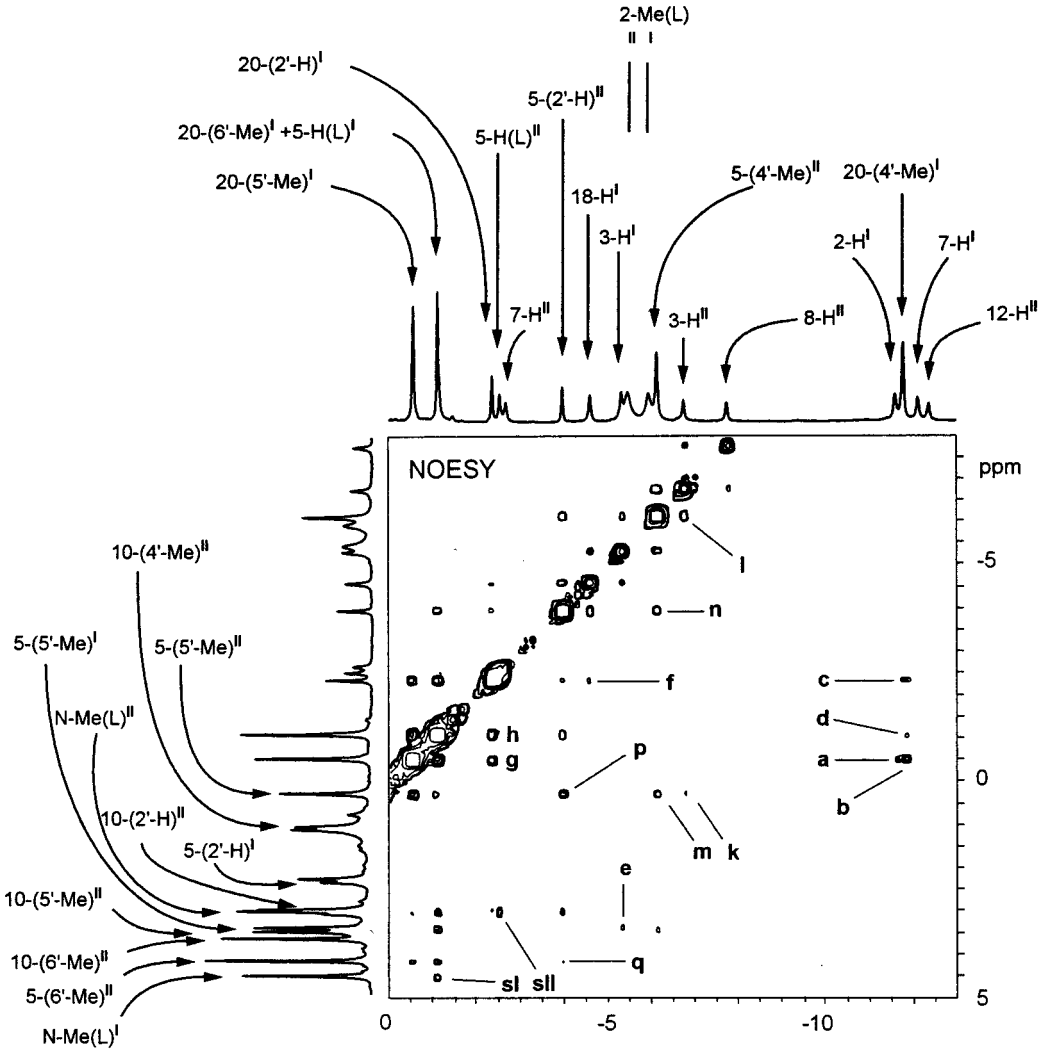

Figure 9. 2D ^{1}H NOESY map spectra of $[(TMCP)Fe^{III}(1,2\text{-diMeIm})_2]^+$ in dichloromethane-d_2 at 190 K. The most characteristic NOE cross-peaks are labeled as follows: **a**, 2-H^I−20-(5′-Me)^I; **b**, 15-(4′-Me)^I−15-(5′-Me)^I; **c**, 15-(2′-H)^I−15-(4′-Me)^I; **d**, 15-(6′-Me)^I−15-(5′-Me)^I; **e**, 3-H^I−5-(5′-Me)^I; **f**, 18-H^I−20-(2′-H)^I; **g**, 15-(2′-H)^I−15-(5′-Me)^I; **h**, 15-(2′-H)^I−15-(6′-Me)^I; **k**, 3-H^{II}−5-(5′-Me)^{II}; **l**, 3-H^{II}−5-(4′-Me); **m**, 20-(4′-Me)^{II}−20-(5′-Me)^{II}; **n**, 20-(2′-H)^{II}−20-(4′-Me)^{II}; **p**, 20-(2′-H)^{II}−20-(5′-Me)^{II}; **q**, (2′-H)^{II}−20-(6′-Me)^{II}. Two other NOE cross-peaks (**sI** and **sII**) between N-Me and 2-Me of the coordinated ligand were observed for isomers *I* and *II*, respectively.

factors which are instrumental in determination of the core geometry demonstrated that ligand−porphyrin nonbonding interactions including *meso*-substituents are the primary determinant of core conformation.[30]

Electronic Structure of Low-Spin Iron(III) Chiroporphyrins. The separation of the dipolar and contact shifts, which is necessary to elucidate the details of the electronic structure using the isotropic shifts, by a typical route for tetrarylporphyrins systems is not accessible for $(TMCP)Fe^{III}X_2$ as the *meso* groups are flexible and paramagnetically shifted due to a less predictable σ-delocalization mechanism. It has been demonstrated that the major contribution to the isotropic shift of the pyrrole protons of low-spin tetrarylporphyrins is of contact origin.[18,19] For bis(imidazole) complexes with the $(d_{xy})^2(d_{xz}d_{yz})^3$ ground state it constitutes ca. 20% of the isotropic shift and produces an upfield shift for the pyrrole and *meso*-substituent resonances but definitely a strong downfield shift for the axially coordinated imidazoles.[18] The $[(TPP)Fe^{III}(CN)_2]^-$ complexes presented a very small dipolar contribution. Generally the negligible dipolar shift was determined for iron porphyrin systems with the pure $(d_{xz}d_{yz})^4(d_{xy})^1$ ground state.[23−25] Thus the contribution of the dipolar shift in the isotropic shift of $[(TMCP)Fe^{III}X_2]$ may be expected to increase in the axial ligand series CN^- (CD_3OD) < CN^- (CD_2Cl_2) < 2-MeImH, 1,2-diMeIm < 1-MeIm, ImH. In the limits of the dipolar shifts expected for two extreme ground states, we have come to conclusion that the isotropic shift pattern reflects mainly the spin density distribution due to the contact mechanism. However, the large difference of the isotropic shifts determined for 4′-Me of $[(TMCP)Fe^{III}(1,2\text{-diMeIm})_2]^+$ but not for $[(TMCP)Fe^{III}(1\text{-MeIm})_2]^+$ is due to the dipolar mechanism and reflects an arrangement of the particular *meso*-alkyl group with respect to the shielding−deshielding zones of the complex as regulated by the steric interaction with the axial ligand.

Generally the ground state of the low-spin iron(III) porphyrin can be described by two limiting electronic configurations:[21−26] $(d_{xy})^2(d_{xz}d_{yz})^3$ and $(d_{xz}d_{yz})^4(d_{xy})^1$ clearly distinguishable by ^{1}H NMR spectroscopy.[18,23−25] In the first case one can expect the upfield position of the pyrrole resonances due to P → Fe delocalization through the $3e_g(\pi)$ filled orbitals of porphyrins. In the second case, the specific downfield position of the pyrrole resonances and strong contact shift of the *meso* substituents are expected. Such a spin density distribution including the large spin density at *meso* positions is indicative of the $(d_{xz}d_{yz})^4(d_{xy})^1$ electronic state with the partial a_{2u} π-cation radical character.[18,23b] In the particular case of the TMCP ligand, the large spin density at *meso* positions will translate into the unusually large downfield shift of the corresponding resonances. Theoretically the contact shift of methine proton equals $Q(\cos^2\theta)\rho/K$, where Q and K are constants and π is π spin density at a *meso* carbon.[41]

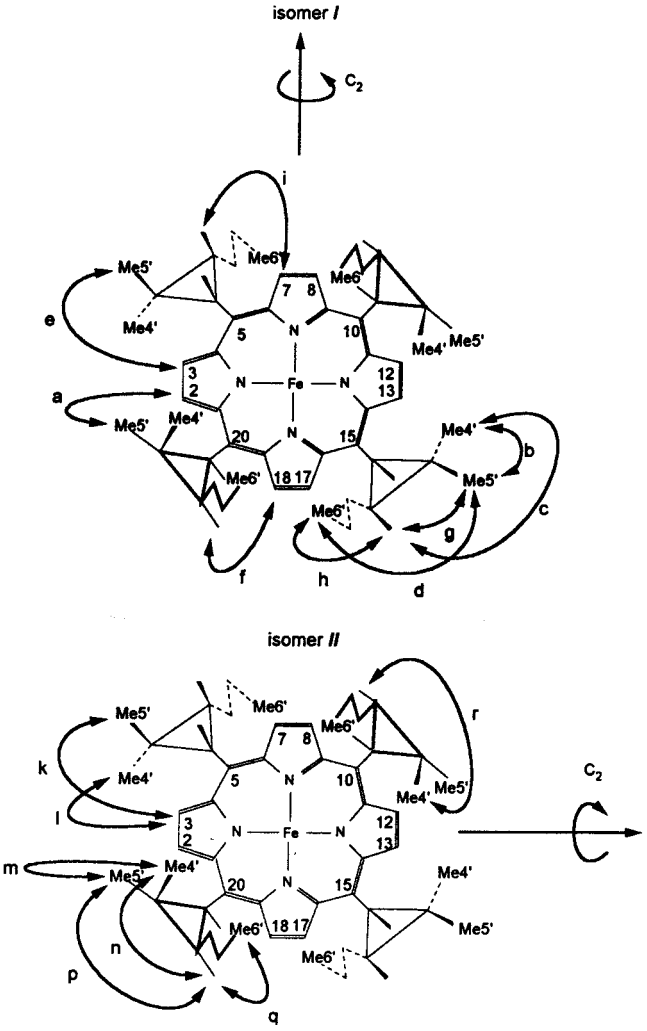

Figure 10. Established NOE connectivities (solid arrows) for two isomers of $[(TMCP)Fe^{III}(1,2\text{-diMeIm})_2]^+$.

Hence the shift value depends also on the specific orientation with respect to the porphyrin macrocycle. This orientation is conveniently described by a dihedral angle between the plane determined by the p_z axis of the *meso* carbon (C_{meso}) and the $C_{meso}-C_1$ bond and the $C_{meso}-C_{1'}-H$ bonds. The value of θ measured from the models approaches 0° for all investigated species as required by the tendency of the bulky *meso* alkyl fragment to be located furthest away from the porphyrin plane. Consequently the position of the 1′-H resonances reflects primary the effects which are related to changes of the spin density accompanying the modification of the ground electronic state. We have noticed the interesting relation between the isotropic shifts of the 1-H′ and pyrrole protons. In general the large downfield isotropic shift of the 1′-H protons was accompanied by smaller upfield shift (as far as the absolute value is concerned) of the pyrrole protons and smaller spread of R-imidazole resonances.

In the $(TMCP)Fe^{III}X_2$ series we have encountered two examples relevant to the two extreme ground electronic states $(d_{xy})^2(d_{xz}d_{yz})^3$, $[(TMCP)Fe^{III}(1\text{-MeIm})_2]^+$ or even better $[(TMCP)Fe^{III}(CD_3OD)_2]^+$,[31] and $(d_{xz}d_{yz})^4(d_{xy})^1$, $[(TMCP)Fe^{III}(CN)_2]^-$ in methanol. The ^1H NMR patterns of the low-spin 2-MeImH or 1,2-diMeIm complexes corresponds to the intermediate situation where both electronic structures are of comparable importance.

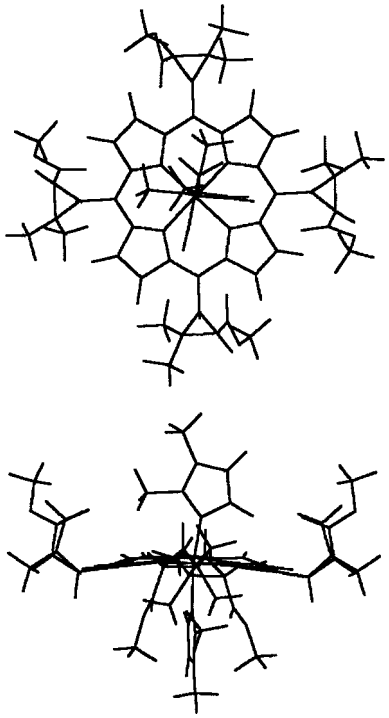

Figure 11. Drawing of the $[(TMCP)Fe^{III}(1,2\text{-diMeIm})_2]^+$ structure obtained from molecular mechanics calculation for the suggested intermediate of the rearrangement process. The porphyrin ring is alternatively ruffled with respect to the primary geometry shown at Figure 1. As the fence is enlarged only on one face of the porphyrin, the placement of the ligand closer to the the *meso* substituent has been accompanied by the displacement of the chiral alkyl substituent outward of the porphyrin pocket. Consequently it extends the diameter of the coordination center and releases the steric congestions.

The curvature of the plots of isotropic shifts vs T^{-1}, particularly for the most sensitive 1′-H resonances and including anti-Curie behavior for $[(TMCP)Fe^{III}(1\text{-MeIm})_2]^+$, can be accounted for by the complex electronic structure of the investigated species (Figure 5). In the simplest description of the electronic structure, the populations of $(d_{xy})^2(d_{xz}d_{yz})^3$ and $(d_{xz}d_{yz})^4(d_{xy})^1$ electronic states vary according to the Boltzmann distribution. Generally in the two-level cases the dependence of isotropic shift on T^{-1} tends toward straight line with the average slope of ground and excited states. At the low-temperature limit the temperature dependence is mainly determined by the ground state. Between the two extreme straight line limits the T^{-1} plot deviates in general from the Curie law.[42] So assuming the $(d_{xz}d_{yz})^4(d_{xy})^1$ ground electronic state for $(TMCP)Fe^{III}(CN)_2$, one may expect that primary linear dependence of the isotropic shift versus T^{-1} will deviate toward upfield direction due to the thermal equilibrium with the $(d_{xy})^2(d_{xz}d_{yz})^3$ excited electronic state. Contrary, the deviation toward downfield direction, determined for $[(TMCP)Fe^{III}(1\text{-MeIm})_2]^+$, implies the $(d_{xz}d_{yz})^4(d_{xy})^1$ excited state.

The intermediate values of the 1′-H and pyrrole isotropic shifts and the deviations from the Curie behavior observed for the sterically hindered imidazole complexes concur with the above discussed electronic structure, assuming that they do correspond to the situation where the populations of both electronic states are comparable. Finally the contribution of the d_{xy} state may be qualitatively probed by the analysis of the isotropic shift of the imidazole ligands. It has been demonstrated that the contact shift results from the Im → Fe π bonding and is effective when the d_π orbitals contain an unpaired electron, i.e. for the $(d_{xy})^2(d_{xz}d_{yz})^3$ configuration.[18] On the other

(41) Pignolet, L. H.; La Mar, G. N. In *NMR of Paramagnetic Molecules*; La Mar, G., Horrocks, W. D., Jr., Holm, R. H., Eds.; Academic Press: New York, 1973; p 357.

(42) Shokiriev, N. V.; Walker, F. A. *J. Phys. Chem.* **1995**, *99*, 17795.

hand, the unpaired spin density cannot be directly transferred into the imidazole fragment if the $(d_{xz}d_{yz})^4(d_{xy})^1$ distribution is operating. Therefore, the small isotropic shifts of bulky imidazoles reflect a significant contribution of the $(d_{xz}d_{yz})^4(d_{xy})^1$ electronic state.

Conclusion. Low-spin iron(III) chiroporphyrin complexes exhibit considerably different properties in relation to analogous low-spin iron(III) tetrarylporphyrins. One can search for the reason of the observed behavior. In the first place the electronic effect of the replacement of the aryl substituents by alkyl groups seems to be crucial. The importance of this factor is well illustrated by the upfield pyrrole shifts of cyanide complexes observed in this investigation, whereas a downfield shift has been determined for $[(TPP)Fe^{III}(CN)_2]^-$. In the case of the R-imidazole ligands the impact of porphyrin ruffling is of importance. The $(TMCP)Fe^{III}$ fragment presented some tendency to assume the S_4 type distortion of the porphyrin core even if ligands are cylindrical. However the steric bulkiness of at least 1,2-diMeIm is required to freeze a favorable configuration, even at room-temperature conditions providing the perpendicular orientation of two imidazole planes which seems to be instrumental[23] in the stabilization of the rare $(d_{xz}d_{yz})^4(d_{xy})^1$ electronic state.

Experimental Section

Materials. $(TMCP)Fe^{III}Cl$ was prepared by iron insertion into $TMCPH_2$[6] using known procedures.[20] Imidazole (ImH), 2-methylimidazole (2-MeImH), 1-methylimidazole (1-MeIm), 1,2-dimethylimidazole (1,2-diMeIm), and tetrabutylammonium cyanide ((TBA)CN) were used as received from Aldrich. Methanol-d_4 (Glaser AG) was used as received. Chloroform-*d* (Glaser AG) and dichloromethane-d_2 (Aldrich) were dried before use by passing through basic alumina.

The dicyano-ligated complexes of the investigated iron(III) porphyrin were prepared by dissolution of 2−3 mg of the respective high-spin complex in 0.4 mL of methanol-d_4 saturated with KCN. The titration of 2−3 mg of $(TMCP)Fe^{III}Cl$ in the respective solvent with nitrogen bases or (TBA)CN was applied to generate low-spin complexes.

NMR Experiments. ^{1}H NMR spectra were recorded on a Bruker AMX spectrometer operating in the quadrature mode at 300 MHz. The residual ^{1}H NMR resonances of the deuterated solvents ($CHCl_3$ or CHD_2OD) were used as a secondary reference. Magnitude COSY spectra were obtained after collecting the standard 1D reference spectra. The 2D COSY spectra were usually collected by use of 1024 points in t_2 over the desired bandwidth (to include all desired peaks) with 512 t_1 blocks and 40−200 scans per block in which 4 dummy scans were included. The repetition time was 200 ms in all cases. Prior to Fourier transformation, the 2D matrix was multiplied in each dimension with a 30° shifted sine-bell squared window function and zero filled to obtain a 1024 × 1024 word square matrix. The NOESY (NOESYTP) were accumulated by use 512 points in t_2 and 1024 in t_1 and 32 scans per t_1 block. Prior to Fourier transformation the 2D matrix was multiplied in each dimension with a 30° shifted sine-bell squared window function and zero-filled to obtain a 1024 × 1024 word square matrix. Experimental parameters were varied to obtain the best resolution and the signal to noise mode. Usually the repetition time was equal to 200 ms. The mixing time was varied in the 15−150 ms range. The NOESY spectra were processed in the phase-sensitive or magnitude modes.

Molecular Mechanics Calculations. Molecular mechanics calculations using the HyperChem software (Autodesk) were carried out and displayed on a PC 486 computer. The standard MM+ force field, with the constrains set on the coordination bonds to achieve a low-spin iron(III) porphyrin geometry, has been used as described in the text.

Acknowledgment. We thank Patrick Dubourdeaux for help with the synthesis of (TMCP)FeCl. The financial support of the State Committee for Scientific Research KBN (Grant 2 2651 92 03 to L.L.-G.) and of the Centre National de la Recherche Scientifique (Grant URA 1194 to J.-C.M.) is kindly acknowledged.

IC970513F